2024 IEEE/RSJ International Conference on Intelligent Robots and Systems (IROS)
October 14-18, 2024. Abu Dhabi, UAE

Dynamic Model and Experimental Validation of a Haptic Robot based on a Flexible Antenna mounted on an Omnidirectional Platform

Luis Mérida-Calvo[1], María Isabel Haro-Olmo[1] and Vicente Feliu-Batlle[2]

Abstract— **The development of new measurement systems for mobile robots has been a growing interest in recent years, particularly tactile systems based on bioinspired sensor antennae, such as whiskers and antennae found in animals and insects. This work focuses on studying a mobile robot equipped with such systems. Specifically, a dynamic model is developed for an omnidirectional robot with a sensing antenna, considering the planar motion of the system and taking into account the gravity effect. The extended Hamilton principle is applied to derive the equations of motion for the mobile platform, while the boundary-value problem is formulated for the antenna. Subsequently, modal analysis is employed to obtain a unique solution for the sensor antenna model, which is then validated using experimental data.**

I. INTRODUCTION

Haptic technology is a field of study that began to be explored in the 1990s [1]. It has been the subject of research in robotics in recent years for the development of various haptic measurement systems, such as whisker-type systems [2] or antenna-type systems [3], with the aim of performing inspection and recognition tasks. Compared to other technologies such as LiDAR, camera vision systems or ultrasonic sensors, haptic technology offers better results in inspection tasks that need to be carried out in environments with poor visibility, due to smoke, humidity, or suspended particles. Furthermore, haptics provides additional information, such as surface rugosity and mechanical impedance, that vision-based systems might miss.

We are developing a prototype called Mobile Robotic Haptic System (hereafter denoted as MRHS) which consists of an omnidirectional mobile platform equipped with a robotic haptic antenna system. It has been previously presented in [4], [5]. The platform is equipped with four motors that drive four omnidirectional wheels, providing the system with the ability to move in all three degrees of freedom independently on the ground (holonomic system). A robotic antenna is mounted on it, consisting of a slender flexible rod, two motors (providing azimuthal and attitude degrees of freedom) and a force-torque sensor. This haptic measurement system has been previously developed in [6]. The objective is to perform recognition tasks while the robot navigates through a specific environment, moving freely using the platform and taking haptic measurements with the antenna.

The antenna equipped in the system is a slender, lightweight carbon fiber rod, designed to minimize the effort required by the motors to execute fast and precise movements. Due to its flexible and lightweight nature, any slight movement induces vibrations. These vibrations are amplified when antenna movements are combined with the movement of the mobile platform. This vibration introduces imprecision in determining the position of the tip of the antenna, thereby hindering the precise reaching of a target and the performance of recognition tasks. Consequently, obtaining a dynamic model that accurately reproduces the antenna's displacement and vibrations is crucial for designing a position control system capable of precisely positioning the tip and eliminating undesired vibrations.

Modeling the dynamics of the proposed sensing antenna is equivalent to that of a flexible link whose base is moved. This problem has been approached using several techniques, as seen in [7]. Focusing on studies that obtain the model of the flexible link considering its continuous nature, some authors consider a single rigid motion at one end of the link. For example, in [8], [9], a rotation at the base is considered, while a translation motion is defined in [10], [11]. Rotation motion and translation at the base are considered simultaneously in [12]. A problem similar to the one addressed in this article is studied in [13], where three degrees of freedom are considered at the base of the link. However, they only formulate the boundary condition problem of the link, which has a mass at the tip and is excited by a distributed force. On the other hand, [14] considers the same number of degrees of freedom including a mass at the end of the link too but, in this model, both transverse and axial deflection in the horizontal plane are studied neglecting the effect of gravity.

In this work, the dynamic model of the system comprising the mobile platform with the haptic system is developed and validated experimentally. The considered motion is restricted to the vertical plane (longitudinal and vertical translations and antenna rotation), including the gravity effect. This motion is a simplification of the real system, which, as mentioned earlier, has 3 degrees of freedom for the platform and 2 for the rotation of the antenna, but it includes the most characteristic issues required to model the real system. Compared with the studies mentioned above, this work advances the state of the art by considering three degrees of freedom, the gravity effect, the dynamics of the entire system (including robot actuators) and experimentally validating the resulting model. For this development, the extended Hamil-

*This work was not supported by any organization

[1]Luis Mérida-Calvo and María Isabel Haro-Olmo are with Instituto de Investigaciones Energéticas y Aplicaciones Industriales (INEI), University of Castilla-La Mancha (UCLM), 13071 Ciudad Real, Spain luis.merida@alu.uclm.es; misabel.haro@alu.uclm.es

[2]Vicente Feliu-Batlle is with Escuela Técnica Superior de Ingeniería Industrial de Ciudad Real (ETSII), University of Castilla-La Mancha (UCLM), 13071 Ciudad Real, Spain vicente.feliu@uclm.es

TABLE I

COMPARISON BETWEEN PRESENT WORK AND PREVIOUS STUDIES

Collected studies	*DOF* considered	Gravity effect	Actuator's dynamics	Experimental validation
[8]	1	×	×	✓
[9]	1	✓	×	×
[10]	1	×	×	×
[11]	1	×	✓	✓
[12]	2	×	×	×
[13]	3	×	×	×
[14]	3	×	×	×
This work	3	✓	✓	✓

ton principle is applied, obtaining the dynamic equations of the entire system and setting the formulation of the boundary conditions to solve the partial differential equation (PDE) that models the antenna. Subsequently, this PDE is solved along with the boundary conditions, also known as the boundary-value problem. Table I summarizes the comparison between the related studies and the present work.

II. ROBOT SETUP

The omnidirectional robot is equipped with four Mecanum wheels, also known as Swedish wheels, with rollers set at 45º. These wheels grant the robot the capability to move independently in any direction on the ground. However, while in motion, the wheels introduce a significant undesired vertical vibration due to the gaps between the rollers. As the motor of each wheel rotates, it causes the wheel to turn, resulting in the rollers making contact with the ground sequentially and inducing a slight vertical displacement. This disturbance is then transmitted through the platform to the antenna, causing it to vibrate. The impact of this phenomenon on the antenna depends on the angular velocity of the motors and the phase difference between the angles of each wheel.

Simulating this phenomenon and comparing it to real experimental data is exceptionally challenging because each wheel exhibits its own backlash, resulting in varying phases between motors. To resemble this phenomenon consistently during experiments, a new set of wheels has been designed. These wheels are circular structures that lack rollers but but feature an eccentric axle. This eccentricity induces a vertical movement in the platform (similar to cam mechanisms) that is easily reproducible both in experimentation and simulations, facilitating the model validation. This design exaggerates the behavior of omnidirectional wheels rather than replicating it.

Thus, the MRHS with eccentric wheels is shown in Figure 1. It equips four DC motors with $1:75$ reduction gears and incremental encoders with $\pm 1.2^\circ$/pulse precision for the eccentric wheels. Driving the haptic system (sensing antenna) there are two harmonic drive DC mini-servo actuators PMA-5A motor sets that include zero backlash 1:50 reduction gears and incremental encoders with $\pm 0.007^\circ$/pulse precision. The haptic system is composed of a slender carbon-fibre rod (the antenna) attached to a six-axis force-torque (FT) sensor ATI FTD-MINI40. The inner current loop of each motor is controlled by Maxon ESCON Module 24/2 servo controller boards. All the system is controlled by a National Instruments Field-Programmable Gate Array (FPGA) Compact RIO control board (sbRIO-9631), powered up by a 22.2V LiPo battery and communicated via WiFi Router to a host computer. This control board is responsible for reading the encoders and the FT sensor, as well as sending control signals to the servo controllers of the motors, operating with a period of 10 ms. In addition, the control board feeds back the encoder signals to implement closed-loop position controls of each motor.

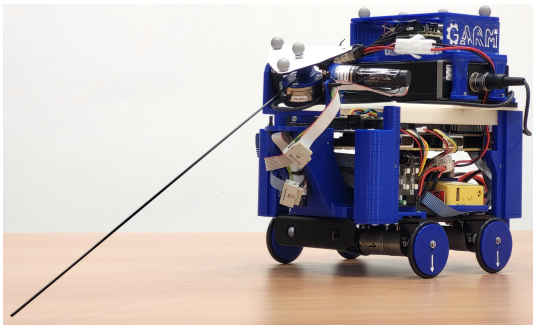

Fig. 1. MRHS equipped with eccentric wheels

III. SYSTEM MODELLING

Figure 2 schematizes the MRHS system. All movements of the system are constrained to the vertical plane defined by the inertial system (X_0, Z_0). The mass of the entire system (omnidirectional platform plus antenna system) is M_b and displaces along the X_0 axis due to the rotation of the wheels, denoted as $\theta_w^i(t)$, caused by the motor torques $\Gamma_w^i(t)$ applied to each wheel by its respective motor. Each motor/wheel is denoted as $i = 1$ (Front-Left), $i = 2$ (Front-Right), $i = 3$ (Back-Left) and $i = 4$ (Back-Right). These motor torques collectively produce the applied horizontal force $F_a(t)$. Each wheel has radius R and is attached to the motor rotating axle with an eccentricity denoted as e, causing a vertical displacement of the robot along the Z_0 axis. Considering gravity g effects, a reaction force appears between the system and the ground, denoted as $F_r(t)$. Furthermore, the haptic system, composed of an antenna attached to a motor, is placed in front of the platform at a distance d and an angle α with respect to the center of mass. The antenna is modeled as a flexible link of length L, linear density ρ, Young's modulus E and area moment of inertia I. The motor of the antenna has a rotational inertia J_a and produce a torque $\Gamma_a(t)$.

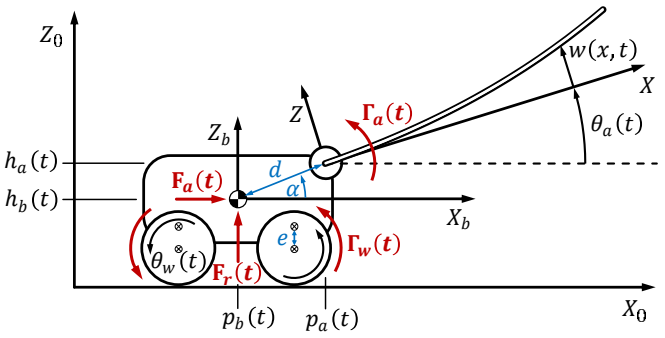

Fig. 2. System Scheme

The following reference frames or coordinate systems are considered: an inertial system (X_0, Z_0) and two non-inertial systems, (X_b, Z_b) and (X, Z). The inertial frame is defined such that Z_0 has the opposite direction to gravity g. The system (X_b, Z_b) is fixed to the platform and placed at the center of mass of the MRHS, while the system (X, Z) is defined at the center of the antenna's motor axle, oriented in such a way that the X axis is aligned with the antenna without deformation (as a rigid link). The horizontal displacements of (X_b, Z_b) and (X, Z) with respects to (X_0, Z_0) are defined as $p_b(t)$ and $p_a(t)$ respectively, and the vertical displacement as $h_b(t)$ and $h_a(t)$. The angle between (X_b, Z_b) and (X, Z) corresponds to the motor angle, defined as $\theta_a(t)$, being positive angles defined as anticlockwise.

Concerning the (X, Z) frame, the deflection of the link due to its flexibility is defined as $w(x,t)$. This deflection consist in the distance from any point x of the link to the frame (X, Z) in the Z direction at the instant t. In this way, the movement with respect to (X, Z) is similar to a cantilever beam. Furthermore, an hypothesis is made in which the deflection $w(x,t)$ of the antenna is described by the Euler-Bernoulli beam theory [15] under the following assumptions:

1) The material of the link is isotropic, homogeneous, and exhibits linear elastic behavior.
2) The deflection $w(x,t)$ is small compared to x, so that $\arctan\left(\frac{w(x,t)}{x}\right)$ is approximated as $\frac{w(x,t)}{x}$.
3) The lateral deflection (produced outside the vertical plane) is not considered.
4) The cross-section of the link remains flat and perpendicular to its axis after deformation.

In addition, due to the first assumption, a first-order analysis can be conducted [16]. Thus, the forces acting are considered on the undeformed link, and the principle of superposition is applied. Moreover, internal and external frictions of the link are not considered.

Some other assumptions regarding the mobile platform are made: (1) the angle between (X_b, Z_b) and (X_0, Z_0) corresponds to the platform pitch angle, which is considered to be constant and equal to zero, (2) the robot moves due to the torques applied by each motor to its respective wheel, assuming perfect grip between the wheels and the ground, so no sliding nor skipping are considered, and (3) the drag force and rolling resistance are considered negligible.

A. Kinematics

Considering the eccentric wheels, the kinematics of the robotic platform is:

$$p_b(t) = -\theta_w(t) \cdot R + e \cdot \cos(\theta_w(t) + \varphi) \tag{1}$$

$$h_b(t) = R + e \cdot \sin(\theta_w(t) + \varphi) \tag{2}$$

being φ the phase of the wheel. Based on (1) and (2) the following vectors with respect to the frame (X_0, Z_0) can be defined:

$$\mathbf{r}_b(t) = \begin{bmatrix} p_b(t) \\ h_b(t) \end{bmatrix} \tag{3}$$

$$\mathbf{r}_a(t) = \mathbf{r}_b(t) + d \begin{bmatrix} \cos(\alpha) \\ \sin(\alpha) \end{bmatrix} = \begin{bmatrix} p_a(t) \\ h_a(t) \end{bmatrix} \tag{4}$$

$$\mathbf{r}_x(x,t) = \mathbf{r}_a(t) + x \begin{bmatrix} \cos(\theta_a(t)) \\ \sin(\theta_a(t)) \end{bmatrix} + w(x,t) \begin{bmatrix} -\sin(\theta_a(t)) \\ \cos(\theta_a(t)) \end{bmatrix} \tag{5}$$

where $\mathbf{r}_b(t) \in \Re^{2\times 1}$ defines the platform center of mass, $\mathbf{r}_a(t) \in \Re^{2\times 1}$ indicates the center of the antenna's motor axle and $\mathbf{r}_x(x,t) \in \Re^{2\times 1}$ defines the position of a differential element of the antenna at a point x relative to the coordinate system (X_0, Z_0). Finally, Equation (5) determines the kinematics describing the movement of the tip of the antenna $[p_t(t), h_t(t)]^\intercal = \mathbf{r}_t(t) = \mathbf{r}_x(L,t)$.

B. Dynamics

1) Obtaining the system equations of motion: The dynamic equations of the system are obtained by applying the Hamilton principle [17], [18], which can be expressed as:

$$\int_{t_1}^{t_2} (\delta T - \delta V + \delta W)\, \mathrm{d}t = 0 \tag{6}$$

where δW is the virtual work produced by the applied forces, and δT and δV are the variation in kinetic and potential energy, respectively. These variations are obtained with respect to the following generalized coordinates: $p_b(t)$, $h_b(t)$, $\theta_a(t)$ and $w(x,t)$.

First of all, the kinetic energy of the system is calculated. Considering vectors (3), (4) and (5), the kinetic energy of the system is obtained operating the following expression:

$$T = \frac{1}{2} M_b \dot{\mathbf{r}}_b^\intercal(t) \cdot \dot{\mathbf{r}}_b(t) + \frac{1}{2} J_a \dot{\theta}_a^2(t) + \frac{1}{2} \int_0^L \rho \dot{\mathbf{r}}_x^\intercal(x,t) \cdot \dot{\mathbf{r}}_x(x,t)\, \mathrm{d}x \tag{7}$$

where the time derivative is denoted as $\dot{(\,)}$. Here, the first term corresponds to the energy associated with the translation of the platform, the second term corresponds to the rotational energy of the antenna's motor, and the last term corresponds to the movement of the antenna itself.

Regarding potential energy, it is defined as a sum of two components: an elastic one, V_e, due to the flexibility of the antenna, and the other due to gravitational effect, V_g. Considering the hypothesis of the antenna being an Euler-Bernoulli beam, the elastic potential energy of the link can be described by:

$$V_e = \frac{1}{2} \int_0^L EI \left(w''(x,t)\right)^2 \mathrm{d}x \tag{8}$$

where $(\,')$ indicates the derivative with respect to the variable x of the frame (X, Z).

The gravitational potential energy of the antenna is defined with respect to the undeformed link, as per the assumption of the first-order analysis:

$$V_g = g M_b h_b(t) + \int_0^L g\rho \left(h_b(t) + d\sin(\alpha) + x\sin(\theta_a(t))\right) \mathrm{d}x \tag{9}$$

where the first term corresponds to the mobile platform and the second one to the antenna.

Finally, work variation is defined as:

$$\delta W = F_a(t)\delta p_b(t) + F_r(t)\delta h_b(t) + \Gamma_a(t)\delta\theta_a(t) - \int_0^L g\rho\cos(\theta_a(t))\delta w(x,t)\,\mathrm{d}x \quad (10)$$

where the first three terms represent the work generated by the forces $F_a(t)$, $F_r(t)$, and the torque $\Gamma_a(t)$. The last term reflects the work generated by gravity in relation to the displacement of the antenna.

When calculating the variation of energies and applying Equation (6), an equation dependent on the virtual displacements of the generalized coordinates $\delta p_b(t)$, $\delta h_b(t)$, $\delta\theta_a(t)$, and $\delta w(x,t)$, and the spatial derivative $\delta w'(x,t) = \frac{\partial}{\partial x}[\delta w(x,t)]$, is obtained.

On one hand, by assuming that the displacements $\delta p_b(t)$, $\delta h_b(t)$, and $\delta\theta_a(t)$ are arbitrary, the sum of their coefficients must be equal to zero. Thus, three equations are obtained that model the dynamics of the mobile platform and the motor that moves the antenna:

$$\begin{aligned}&(M_b+\rho L)\,\ddot{p}_b(t) - \rho\int_0^L \ddot{w}(x,t)\,\mathrm{d}x\sin(\theta_a(t))\\ &-\rho\left(\frac{L^2}{2}\sin(\theta_a(t)) + \int_0^L w(x,t)\,\mathrm{d}x\cos(\theta_a(t))\right)\ddot{\theta}_a(t)\\ &-\rho\left(\frac{L^2}{2}\cos(\theta_a(t)) - \int_0^L w(x,t)\,\mathrm{d}x\sin(\theta_a(t))\right)\dot{\theta}_a^2(t)\\ &-\rho\int_0^L \dot{w}(x,t)\,\mathrm{d}x\,\dot{\theta}_a(t)\cos(\theta_a(t)) = F_a(t)\end{aligned} \quad (11)$$

$$\begin{aligned}&(M_b+\rho L)\,\ddot{h}_b(t) - \rho\int_0^L \ddot{w}(x,t)\,\mathrm{d}x\cos(\theta_a(t)) + g\,(M_b+\rho L)\\ &+\rho\left(\frac{L^2}{2}\cos(\theta_a(t)) - \int_0^L w(x,t)\,\mathrm{d}x\sin(\theta_a(t))\right)\ddot{\theta}_a(t)\\ &-\rho\left(\frac{L^2}{2}\sin(\theta_a(t)) + \int_0^L w(x,t)\,\mathrm{d}x\cos(\theta_a(t))\right)\dot{\theta}_a^2(t)\\ &-\rho\int_0^L \dot{w}(x,t)\,\mathrm{d}x\,\dot{\theta}_a(t)\sin(\theta_a(t)) = F_r(t)\end{aligned} \quad (12)$$

$$\begin{aligned}&\left(J_a+\rho\frac{L^3}{3}\right)\ddot{\theta}_a(t) + \rho\int_0^L x\ddot{w}(x,t)\,\mathrm{d}x + g\rho\frac{L^2}{2}\cos(\theta_a(t))\\ &-\rho\left(\frac{L^2}{2}\sin(\theta_a(t)) + \int_0^L w(x,t)\,\mathrm{d}x\cos(\theta_a(t))\right)\ddot{p}_b(t)\\ &+\rho\left(\frac{L^2}{2}\cos(\theta_a(t)) - \int_0^L w(x,t)\,\mathrm{d}x\sin(\theta_a(t))\right)\ddot{h}_b(t) = \Gamma_a(t)\end{aligned} \quad (13)$$

Equations (11)-(12) describe the movement of the robotic platform meanwhile equation (13) corresponds to the motor of the antenna.

On the other hand, virtual displacement $\delta w(x,t)$ is arbitrary over the domain $0 < x < L$. Thus, the following expression is obtained:

$$\begin{aligned}EIw''''(x,t) + \rho\Big(&\ddot{w}(x,t) + x\ddot{\theta}_a(t) - \ddot{p}_b(t)\sin(\theta_a(t))\\ &+\ddot{h}_b(t)\cos(\theta_a(t))\Big) = -g\rho\cos(\theta_a(t))\end{aligned} \quad (14)$$

which is equivalent to the Euler-Bernoulli beam equation. Furthermore, it is assumed that $\delta w(x,t)$ and $\delta w'(x,t)$ or their respective coefficients are equal to zero at the limits $x = 0$ and $x = L$. Then, the boundary conditions that allow solving equation (14) are obtained:

$$w(0,t) = 0; \quad w'(0,t) = 0 \quad (15)$$

$$w''(L,t) = 0; \quad w'''(L,t) = 0 \quad (16)$$

where (15) corresponds to a fixed beam condition at the base of the antenna and (16) to a free end condition. The set of equations (14)-(16) is known as the boundary-value problem. The solution to this problem results in a set of infinite ordinary differential equations dependent on time that model the behavior of the sensor antenna.

2) Solving the boundary-value problem: Modal analysis for continuous systems [17] is applied in order to obtain the mathematical model that describes the behaviour of the antenna. Therefore, first, the method of separation of variables is applied and the eigenvalue problem is solved. It is assumed that, applying the separation of variables, the deflection can be expressed as:

$$w(x,t) = \sum_{i=1}^{\infty}\psi_i(x)\phi_i(t) \quad (17)$$

where $\psi_i(x)$ are known as characteristic functions or normal modes of a beam, and $\phi_i(t)$ are the harmonic functions of time. The solution of the normal modes is obtained by solving the eigenvalue problem, obtained by applying the relation (17) to equations (14)-(16) and imposing that the external excitations are null. Therefore, the eigenvalue problem is:

$$EI\psi_i''''(x) - \omega_i^2\rho\psi_i(x) = 0 \quad (18)$$

$$\psi_i(0) = 0; \quad \psi_i'(0) = 0 \quad (19)$$

$$\psi_i''(L) = 0; \quad \psi_i'''(L) = 0 \quad (20)$$

where ω_i is the vibration frequency obtained from the following characteristic equation:

$$1 + \cos(\beta L)\cosh(\beta L) = 0 \quad (21)$$

that is solved numerically and have infinite solutions $\beta_i^4 = \frac{\omega_i^2\rho}{EI}$. General solution of (18) is:

$$\begin{aligned}\psi_i(x) = C_{1i}\sin(\beta_i x) + C_{2i}\cos(\beta_i x) +\\ C_{3i}\sinh(\beta_i x) + C_{4i}\cosh(\beta_i x)\end{aligned} \quad (22)$$

where C_{1i}, C_{2i}, C_{3i} y C_{4i} are obtained from the conditions (19)-(20) imposing that the solution of $\psi_i(x)$ is non-trivial. Thus, the following expression is obtained:

$$\begin{aligned}\psi_i(x) = C_{1i}\,&[(\cos(\beta_i x) - \cosh(\beta_i x))\,(\sin(\beta_i L) - \sinh(\beta_i L))\\ &-(\sin(\beta_i x) - \sinh(\beta_i x))\,(\cos(\beta_i L) - \cosh(\beta_i L))]\end{aligned} \quad (23)$$

where C_{1i} is calculated using the orthonormality condition:

$$\rho\int_0^L \psi_i(x)\psi_j(x)\mathrm{d}x = \frac{EI}{\omega_i^2}\int_0^L \psi_i''(x)\psi_j''(x)\mathrm{d}x = \Delta_{ij} \quad (24)$$

being Δ_{ij} the Kronecker delta and $i, j = 1, 2, \ldots, \infty$.

After solving the eigenvalue problem, the solution to equation (14) is derived using the expansion theorem, resulting in a set of uncoupled ordinary differential equations in terms of $\phi_i(t)$:

$$\sum_{i=1}^{\infty} \Delta_{ij}\left(\ddot{\phi}_i(t) + \omega_i^2 \phi_i(t)\right) = -\rho \int_0^L x\psi_j(x)\,\mathrm{d}x\,\ddot{\theta}_a(t) \qquad (25)$$
$$-\rho \int_0^L \psi_j(x)\,\mathrm{d}x\left(g\cos(\theta_a(t)) + \ddot{h}_b(t)\cos(\theta_a(t)) - \ddot{p}_b(t)\sin(\theta_a(t))\right)$$

where $i, j = 1, 2, \ldots, \infty$.

Finally, the dynamic model of the antenna is obtained by truncating the number of vibration modes to n. Thus, defining the vectors $\boldsymbol{\phi}(t) = [\phi_1(t)\ \phi_2(t)\ \cdots\ \phi_n(t)]^\intercal$ y $\boldsymbol{\psi}(t) = [\psi_1(t)\ \psi_2(t)\ \cdots\ \psi_n(t)]^\intercal$ belonging to $\Re^{n\times 1}$, the following expression is obtained:

$$\mathbf{I}\ddot{\boldsymbol{\phi}}(t) + \mathbf{W}\boldsymbol{\phi}(t) = \mathbf{P}\mathbf{u}(t) \qquad (26)$$

where $\mathbf{I} \in \Re^{n\times n}$ is the identity matrix and

$$\mathbf{W} = diag\left(\omega_1^2, \omega_2^2, \ldots, \omega_n^2\right) \in \Re^{n\times n} \qquad (27)$$

$$\mathbf{P} = \rho \int_0^L \left[-x\boldsymbol{\psi}(x) \quad \boldsymbol{\psi}(x) \quad -\boldsymbol{\psi}(x) \quad -g\boldsymbol{\psi}(x)\right] \mathrm{d}x \in \Re^{n\times 4} \qquad (28)$$

$$\mathbf{u}(t) = \begin{bmatrix} \ddot{\theta}_a(t) \\ \ddot{p}_b(t)\sin(\theta_a(t)) \\ \ddot{h}_b(t)\cos(\theta_a(t)) \\ \cos(\theta_a(t)) \end{bmatrix} \in \Re^{4\times 1} \qquad (29)$$

The variables measured from the model are: the coupling torque, measured at the base of the antenna:

$$\Gamma_c(t) = -EIw''(0,t) = -EI\boldsymbol{\psi}''(0)^\intercal\boldsymbol{\phi}(t), \qquad (30)$$

and the deflection of the antenna measured at the tip ($x = L$) with respect to the system (X, Z):

$$w(L,t) = \psi(L)^\intercal\boldsymbol{\phi}(t) \qquad (31)$$

In conclusion, equations (11)-(12) model the dynamic behavior of the mobile platform, (13) represents the equation governing the motor that moves the antenna, and (26) provides an approximation of the antenna's behavior, as it is truncated at n modes. Together, these four equations constitute the dynamic model of the system.

C. DC motors dynamics

The general equation describing the dynamics of any DC motor of the system is:

$$n_j \cdot k_j \cdot V(t) = J_j \cdot \ddot{\theta}_j(t) + \nu_j \cdot \dot{\theta}_j(t) + \Gamma_j^f(t) + \Gamma_j^u(t) \qquad (32)$$

where $\Gamma_j^u(t)$ is the useful or resultant applied torque, n_j is the reduction gear ratio, k_j is the electromechanical constant of the motor servo amplifier system, $V(t)$ is the motor input voltage, $\theta_j(t)$, J_j, ν_j and $\Gamma_j^f(t)$ are the angular position, inertia, viscous friction and nonlinear friction of the motor, respectively, and j denotes the system as $j = w$ (mobile platform motors) and $j = a$ (antenna motor).

The torque $\Gamma_j^u(t)$ can be considered also as the torque employed to move the system driven by the motor. Considering it, along with $\Gamma_j^f(t)$, as disturbances to the system, the Equation (32) can be rewritten to obtain a transfer function between the input voltage and the motor angle taking Laplace transforms:

$$G_j(s) = \frac{\theta_j(s)}{V(s)} = \frac{\frac{n_j \cdot k_j}{J_j}}{s^2 + \frac{\nu_j}{J_j}\cdot s} = \frac{A_j}{s\cdot(s + B_j)} \qquad (33)$$

Assuming perfect grip of the wheels, a displacement of the robot along the X_0 direction implies all four motors turning the same angle, $\theta_w^i(t) = \theta_w(t)$, $\forall i$. Along with this, assuming homogeneity between motors in physical parameters, all motors provide the same amount of torque, $\Gamma_w^i(t) = \Gamma_w(t)$, $\forall i$, being $\Gamma_w(t) = n_w \cdot k_w \cdot V(t)$. Thus, the applied force $F_a(t)$ to the mobile platform can be approximated to:

$$F_a(t) \approx 4 \cdot \frac{\Gamma_w^u(t)}{R} \qquad (34)$$

where R is the radius of the wheels and $\Gamma_w^u(t)$ is the resultant applied torque that can be considered as a disturbance in Equation (32). Thus, the disturbance effect $\Gamma_w^u(t)$ to the system defined by Equation (33) is calculated as:

$$\Gamma_w^u(t) = \frac{F_a(t)\cdot R}{4} \qquad (35)$$

where $F_a(t)$ is the applied force described by Equation (11).

Following the same procedure, the resultant applied torque to the antenna $\Gamma_a^u(t)$ is calculated as:

$$\Gamma_a^u(t) = \Gamma_a(t) - J_a \cdot \ddot{\theta}_a(t) \qquad (36)$$

being $\Gamma_a(t)$ the applied torque to the antenna described by Equation (13). In this case we substract the inertia of the motor from the term because it is already considered in the model of the motor defined by Equation (33).

IV. CONTROL SCHEMES OF THE MOTORS

The control schemes governing the motors of both the mobile platform and the antenna consist in a K_c proportional regulator plus a compensator to overcome nonlinearities affecting each motor. The model scheme of the motors, the process to identify all parameters (including nonlinearities) and the design of the compensator are described in [4], [5]. The parameters of the motors and control loops are indicated in Table II.

TABLE II

PARAMETERS OF THE CONTROL LOOPS OF THE MOTORS

Parameter	Wheel's Motors	Antenna's Motors
A	8.698	11956
B	42.857	200
L (s)	0.020	0.010
V_f^S	340	18
V_f^K	18.6	0
V_{sat}	3567.2	4000
K_c	40	0.45
V_f^{min}	350	0
e_{min} (°)	1.2	0.17

V. MODEL VALIDATION

In this section the dynamic model is validated by comparing simulation and experimental results. The Equations (11), (12), (13) and (26), along with the motor dynamics of (32) and (33) and their respective control schemes, constitute the dynamic model of the entire system. Simulations are conducted in *MATLAB/Simulink*. The dynamics of the mobile platform motor control schemes along with (11) and (12) through (35) and the kinetic Equations (1) and (2) simulate the mobile platform displacement $p_b(t)$, $h_b(t)$ in the (X_0, Z_0) frame. The dynamics of the antenna motor control scheme along with (13) through (36) simulate the motor angle $\theta_a(t)$. Finally, these results are processed through (29) to simulate the movement of the antenna by (26) truncating the number of vibration modes to $n = 4$ (considering a wide range of frequencies), obtaining the coupling torque of the antenna at the base, $\Gamma_c(t)$ (30) and the position of the tip $p_t(t)$, $h_t(t)$ in (X_0, Z_0) through (31) and (5). Table III summarizes the main system parameters involved in these simulations and described in Section III.

TABLE III

SYSTEM CHARACTERISTICS

Parameter	Quantity	Units
M_b	3.50	kg
R	0.0272	m
e	0.005	m
φ	-90	deg
d	0.156	m
α	24.17	deg
L	0.474	m
ρ	5.3×10^{-3}	kg/m
E	1.15×10^{11}	N/m^2
I	7.54×10^{-13}	m^4

A. Design of the trajectories

During a typical recognition task, the MRHS moves forward with determined velocity and acceleration, while the antenna scans the space in front. Considering the physical limitations of the equipment and the maximum accelerations that can be generated, the reference trajectories $p_b^*(t)$ and $\theta_a^*(t)$ are designed. The reference $p_b^*(t)$ consists in a displacement of the mobile platform along X_0. Assuming perfect grip of the wheels, the input trajectory to the control schemes of the mobile platform motors, $\theta_w^*(t)$, is calculated from the reference $p_b^*(t)$ by numerically solving Equation (1). On the other hand, the reference $\theta_a^*(t)$ consists in a rotation of the motor of the antenna, which moves the haptic system in such a way that the antenna sweeps the space in front of the robot. The combination of both references performs an object-searching task, scanning for any object in front of the robot.

B. Simulated and experimental results

Experiments are conducted where the MRHS prototype undergoes the designed references. The experimental data is recorded by various systems. Robot and tip of the antenna positions are measured by an optical camera-based system called *Qualisys*. Angle of the motors are registered by the equipped encoders. Finally, the coupling torque is measured with the FT sensor at the base of the antenna.

Figure 3 represents the results of $p_b(t)$ and $h_b(t)$. Simulation matches experimental data with a root mean square error (RMSE) of just 4.48 mm for $p_b(t)$ and 0.36 mm for $h_b(t)$. These results demonstrate that the controllers of the motor angles are working as planned, even when considering the dynamics of the platform as an input disturbance. Furthermore, the assumption of perfect wheel grip is confirmed, as evidenced by a steady-state error lower than 1%. Thus, the system exhibits no unexpected behavior, such as lateral deflections or platform pitching.

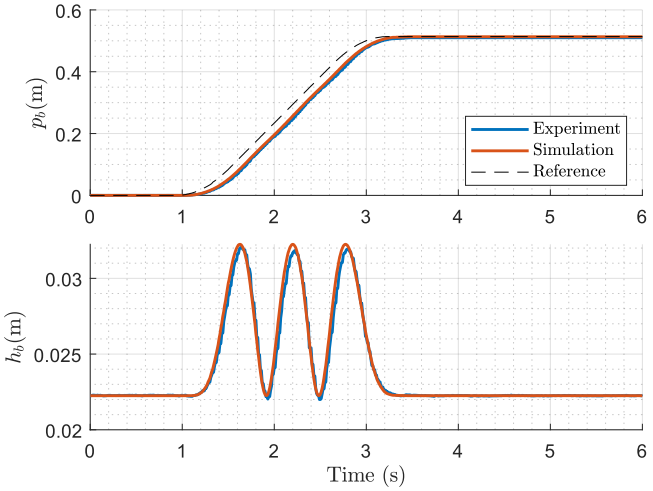

Fig. 3. Simulated an experimental results of $p_b(t)$ and $h_b(t)$

Similarly, Figure 4 plots the results of the antenna motor angle $\theta_a(t)$. The RMSE between simulation and experimental data is just 0.18°, proving the effectiveness of the control scheme.

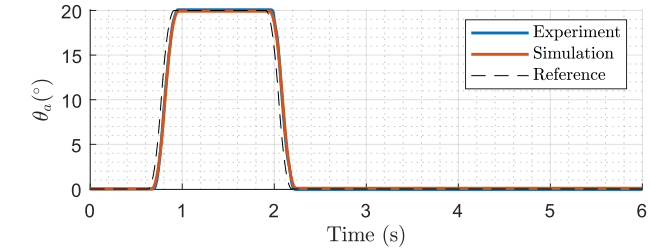

Fig. 4. Simulated an experimental results of $\theta_a(t)$

Figure 5 displays the coupling torque $\Gamma_c(t)$ results. Difference at the beginning between simulation and experiment is due to unnoticeable input reference variations, as the antenna is very sensitive. To evaluate the goodness of this result, the Fast-Fourier transform (FFT) is applied to both simulation and experimental data. It is observed that the first frequency vibration mode of the antenna matches at 10 Hz in both cases, and the second frequency is negligible. This demonstrates that considering more than $n = 1$ vibration modes in (26) to accurately model antenna behaviour is unnecessary.

Finally, Figure 6 depicts the results of the antenna tip positions $p_t(t)$ and $h_t(t)$. In this case, simulation matches experimental data with a RMSE of just 2.88 mm for $p_t(t)$

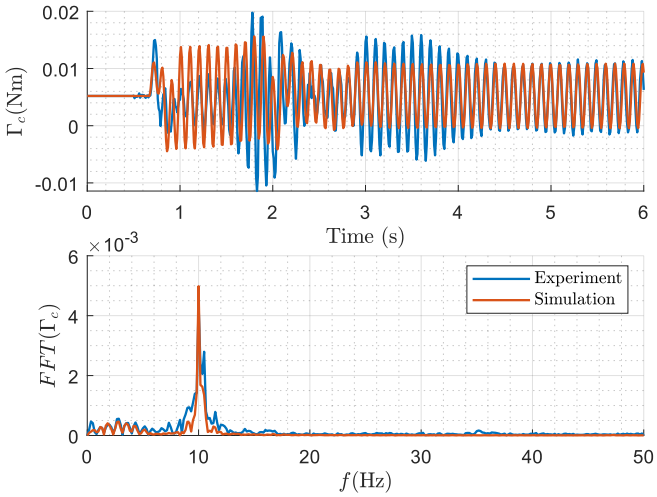

Fig. 5. Simulated an experimental results of $\Gamma_c(t)$, along with each FFT

and 0.64 mm for $h_t(t)$. These results confirm the goodness of the system model, being able to replicate the behaviour of the tip of the antenna accurately.

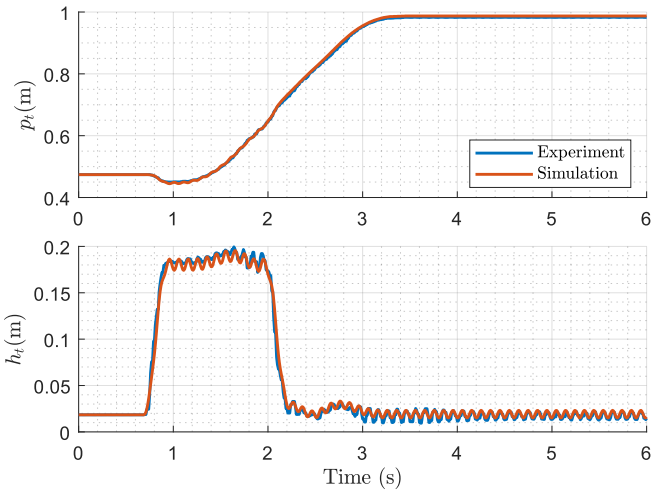

Fig. 6. Simulated an experimental results of $p_t(t)$ and $h_t(t)$

VI. CONCLUSIONS

In this work, the dynamic model of a haptic system composed of an omnidirectional robot and a flexible antenna has been developed. The contribution of this paper has been modelling the interaction between the displacement and vertical oscillation induced by the mobile platform's wheels and the flexible antenna mounted on it. Such oscillation induces a detrimental vibration in the antenna that impedes its use for detection and recognition tasks. Then modelling these dynamics is of paramount importance in order to design a controller that removes such antenna vibrations. Such model has been obtained by applying the extended Hamilton principle and is general in the sense that includes the gravity effect and an arbitrary number of vibration modes of the antenna. This model has been validated by comparing its simulated results with experimental data, proving that considering only one vibration mode is sufficient. Both simulation and experimental results have been obtained using reference trajectories that are designed according to the physical limitations of the system. Our future work is using this model to design a control system that cancels these vibrations.

ACKNOWLEDGMENT

This research was funded in part by the Grant PID2022-141409OB-C21 funded by MCIN/AEI/ 10.13039/ 501100011033 / FEDER "A way of making Europe".

REFERENCES

[1] R. Russell, "Using tactile whiskers to measure surface contours," in *Proceedings 1992 IEEE International Conference on Robotics and Automation*, 1992, pp. 1295–1299 vol.2.

[2] M.-A. Sayegh, H. Daraghma, S. Mekid, and S. Bashmal, "Review of recent bio-inspired design and manufacturing of whisker tactile sensors," *Sensors*, vol. 22, no. 7, 2022.

[3] M. Kaneko, N. Kanayama, and T. Tsuji, "Active antenna for contact sensing," *IEEE Transactions on Robotics and Automation*, vol. 14, no. 2, pp. 278–291, 1998.

[4] L. Mérida-Calvo, A. S. Rodríguez, F. Ramos, and V. Feliu-Batlle, "Advanced motor control for improving the trajectory tracking accuracy of a low-cost mobile robot," *Machines*, vol. 11, no. 1, 2023.

[5] A. Mehallel, L. Mérida-Calvo, R. Rivas-Perez, and V. Feliu-Batlle, "A new smith predictor motor control system to reduce disturbance effects caused by unknown terrain slopes in mobile robots," *Actuators*, vol. 13, no. 2, 2024.

[6] V. Feliu-Batlle, D. Feliu-Talegon, and C. F. Castillo-Berrio, "Improved object detection using a robotic sensing antenna with vibration damping control," *Sensors (Basel, Switzerland)*, vol. 17, no. 28406449, p. 852, Apr. 2017.

[7] D. Subedi, I. Tyapin, and G. Hovland, "Review on Modeling and Control of Flexible Link Manipulators," *Modeling, Identification and Control*, vol. 41, no. 3, pp. 141–163, 2020.

[8] F. Bellezza, L. Lanari, and G. Ulivi, "Exact modeling of the flexible slewing link," in *Proceedings., IEEE International Conference on Robotics and Automation*, 1990, pp. 734–739 vol.1.

[9] N. Mishra, S. Singh, and B. C. Nakra, "Dynamic analysis of a single link flexible manipulator using lagrangian-assumed modes approach," *2015 International Conference on Industrial Instrumentation and Control, ICIC 2015*, pp. 1144–1149, July 2015.

[10] G. Zhu, S. Ge, and T. Lee, "Variable structure regulation of a flexible arm with a translational base," in *Proceedings of the 36th IEEE Conference on Decision and Control*, vol. 2, 1997, pp. 1361–1366 vol.2.

[11] L. Lu, Z. Chen, B. Yao, and Q. Wang, "A two-loop performance-oriented tip-tracking control of a linear-motor-driven flexible beam system with experiments," *IEEE Transactions on Industrial Electronics*, vol. 60, no. 3, pp. 1011–1022, 2013.

[12] S. A. Emam, "Dynamics of a flexible-hub geometrically nonlinear beam with a tip mass," *Journal of Vibration and Control*, vol. 16, no. 13, pp. 1989–2000, June 2010.

[13] A. Tavasoli, "Robust adaptive boundary control of a perturbed hybrid euler-bernoulli beam with coupled rigid and flexible motion," *International Journal of Control, Automation and Systems*, vol. 15, no. 2, pp. 680–688, 2017.

[14] P. Kumar and B. Pratiher, "Position analysis and nonlinear phenomena of flexible manipulator with generic payload mounted on a moving base," *Proceedings of the Institution of Mechanical Engineers, Part K: Journal of Multi-body Dynamics*, vol. 234, no. 2, pp. 408–423, Jan. 2020.

[15] E. Oñate, "Slender plane beams. euler-bernoulli theory," in *Structural Analysis with the Finite Element Method Linear Statics: Volume 2. Beams, Plates and Shells*. Springer Netherlands, 2013, pp. 2–3.

[16] B. Davison and G. Owens, *Steel designers' manual*. Wiley-Blackwell, 2012.

[17] L. Meirovitch, *Analytical Methods in Vibrations*, ser. Macmillan series in applied mechanics. Macmillan, 1967.

[18] ——, *Principles and Techniques of Vibrations*. Prentice Hall, 1997.